MICROWAVE IRRADIATION SYNTHESIS TO OBTAIN $La_{0.7-x}Pr_xCa_{0.3}MnO_3$ PEROVSKITES: ELECTRICAL AND ELECTROCHEMICAL PERFORMANCE

A.C. Ferrel- Alvarez[a], M.A. Domínguez-Crespo[b*], H. Cong[c], A.M. Torres- Huerta[b], D. Palma-Ramírez[d], J. T. S. Irvine[e].

[a]Instituto Politécnico Nacional, CICATA- Altamira, Grupo CIAMS, Km 14.5 Carretera Tampico- Puerto Industrial Altamira, C.P. 89600, Altamira, México e- mail: atzin.ferrel@gmail.com
[b]Instituto Politécnico Nacional, UPIIH, Km 1+500, Carretera Pachuca- Actopan, C.P. 42162, San Agustín Tlaxcala, Hgo, México e-mail: adcrespo2000@yahoo.com.mx
[c]Department of Chemical, Biomolecular and Corrosion Engineering, The University of Akron, Akron, OH, 44325-3906, USA
[d]Instituto Politécnico Nacional, Centro Mexicano para La Producción Más Limpia (CMPL) Av. Acueducto S/N, La Laguna Ticomán, C.P. 07340, Cd. México, México
[e]School of Chemistry, University of St. Andrews, KY16 9ST, Scotland, United Kingdom.

*Corresponding author: mdominguezc@ipn.mx

ABSTRACT

$La_{0.7-x}Pr_xCa_{0.3}MnO_3$ **(LPCM)** perovskites previously synthesized by the microwave-assisted method at 4 minutes and with different stoichiometry (x=0.35, 0.52 and 0.63) were evaluated **through thermogravimetric analysis (TGA)**, **electrical conductivity, thermal expansion coefficient (TEC), scanning electron microscopy (SEM),** Brunauer- Emmet- Teller (BET) **analysis and electrochemical impedance spectroscopy (EIS) using yttria stabilized zirconia (YSZ) as an electrolyte.** The results are discussed in terms of the potential as cathode material to be applied in solid oxide fuel cells (SOFCs) applications at temperatures from 600 to 800 °C. Results derived from TGA showed that Pr promotes the **uncoupling oxygen and** oxygen vacancies favoring the fuel combusting. **Also,** TEC analysis revealed adequate stability **between the YSZ electrolyte and the $La_{0.7-x}Pr_xCa_{0.3}MnO_3$ to avoid cracking or failing,** especially with high amount of Pr. The transition in morphology from **irregular** to **regular** shapes improves the BET and Barret- Joyner- Halenda (BJH) surfaces **and promotes the triple phase boundary (TPB) connectivity**. The electrical conductivity correlated to the **availability in oxygen vacancies showed maximum conductivities in the order of 10^{-2} S cm^{-1}. Activation energy (Ea) was found to be reduced with a minimum quantity of Pr (0.071 eV).** EIS results indicate that the oxygen vacancies **in the LPCM/YSZ system** were better promoted with the highest amount of Pr= 0.63 **(η=0.9 V, 800 °C and 0.06 V of amplitude) in comparison with the minimum, Pr=0.35 (η=1.2 V, 800 °C and 0.06 V of amplitude).**

Keywords: Lanthanum manganites, Microwave irradiation synthesis, Electrical conductivity SOFC cathode materials, Ceramic Interconnects.

1. INTRODUCTION

Solid oxide fuel cells (SOFCs) **are known as a current generation** electrochemical devices **that can produce electrical energy** through of oxidation and reduction reactions [1]. **The SOFCs devices** are considered as a flexible-environmental-friendly solution for the **electric energy generation** from hydrogen, natural gas and other renewable fuels, **giving much higher efficiencies than conventional energy systems [2-8]. The high operation temperature of electrolyte in SOFCs (~900 °C) is an important limitation in commercial applications [9]. For this reason, porous materials with high and stable ionic (10^{-1} -10^{-4} S cm^{-1})/electrical conductivities (higher than 100 S cm^{-1}) at temperatures from 600 °C to 1000°C are desirable as components of the SOFCs [10, 11]. At the same time, environmental regulations demand efficient methods to optimize the different sections that integrate the SOFCs [12, 13]. Therefore, there is a constant interest for the synthesis of new and low cost materials to produce high power densities [14]. Typically, porous cermets of Ni/YSZ are used as anode showing a high catalytic activity during the hydrogen oxidation reaction as well as modular electrical conductivity (100-1700 S cm^{-1}) and excellent good thermal expansion compatibility (11.88 × 10^{-6} K^{-1}) with the YSZ (12.6 × 10^{-6} K^{-1}). YSZ is one of the most used electrolytes because it provides oxygen vacancies positively affecting the ionic and electrical conductivities.**

On the other hand, $La_{1-x}Sr_xMnO_3$ (LSM) perovskites are commonly used as cathode to enhance the kinetics of oxygen reduction reaction (ORR) and the compatibility with the electrolyte [15, 16]. The ORR can only occur at **the triple phase boundaries (TPB) which are defined as the interface between the cathode, the electrolyte and the oxygen gas [17, 18]. In this context, the microstructure and the composition play a key role since they clearly affect the size and distribution of the TPB because the reaction cannot take place if there is a breaking in the connectivity of any of the three boundary phases [19, 20]. Unfortunately, LSM usually requires operating temperatures above 800 °C, which causes its eventual degradation having a strong impact on the performance of the cell [15, 21-23]. Thus, the main problem of the degradation process is the formation of isolated phase (for**

example, $La_2Zr_2O_7$, LZO) that reduces ion conductivity at high temperatures (800 °C-1000 °C) [24, 25]; i.e. it breaks the connectivity in the TPB.

An alternative to modify the microstructure and improve TBP is through doping or cation substitution in either A or B sites of LSM perovskites [19, 26, 27]. The LSM has been doped in the A- site by lanthanide elements (Ce, Pr, Nd, Sm and Gd) or in the B- site (Fe, Cr, Co, Ni and Ti) to reduce the mismatch of the thermal expansion coefficient with either Gd-doped CeO_2 (GDC) or YSZ electrolytes as well as to reduce the polarization resistance of the cell [16, 26, 28-30]. Other elements that can be considered to dope and substitute the cationic site A of ABO_3 perovskites with excellent catalytic activity during oxygen reduction are Pr and Ca [31-33]. In a previous work, we reported the synthesis of $La_{0.7-x}Pr_xCa_{0.3}MnO_3$ (x=0.35, 0.52, 0.63) perovskites using a non-conventional microwave irradiation method where it was found that this method helps to obtain pure phases and that the addition of Pr into manganite structure favors the transformation from cubic to orthorhombic structure [34]. Based on this research, we selected the condition at which the samples displayed the lowest charge transfer resistance at room temperature (4 min of reaction time) to evaluate the electrical and electrochemical performance of the perovskites with different Pr molar mass (x=0.35, 0.52 and 0.63) in the range of temperatures from 600 to 800 °C while determining the role of this element during the ORR and evaluating its potential application for SOFCs.

2. EXPERIMENTAL

2.1 Cathode preparation

The $La_{0.7-x}Pr_xCa_{0.3}MnO_3$ perovskites were prepared using the microwave irradiation method from nitrate compounds. **Lanthanum(III) nitrate hexahydrate ($La(NO_3)_3 \cdot 6H_2O$, 99.99% purity), Praseodymium(III) nitrate hexahydrate ($Pr(NO_3)_3 \cdot 6H_2O$, 99.9% purity), calcium nitrate tetrahydrate ($Ca(NO_3)_2 \cdot 4H_2O$, 99% purity) and manganese(II) nitrate tetrahydrate ($Mn(NO_3)_2 \cdot 4H_2O$, ≥97.0 % purity) were acquired from Sigma Aldrich and then weighed at stoichiometric amounts according to $La_{0.7-x}Pr_xCa_{0.3}MnO_3$ composition (x=0.35, 0.52 and 0.63). The salt mixtures were placed in high alumina crucibles, dissolved in nitric acid (70%) and deionized water. The alumina crucible was covered with a quartz tube and subjected to microwave irradiation in a modified domestic microwave oven with a power of 900 W and radiation frequency of 2.45 GHz** [34]. **The powders were**

synthesized with a reaction time of 4 min, cooled at room temperature (1-3 h) and grounded in an agate mortar. Subsequently, the powders were uniaxially compressed at 528 MPa and sintered at 1100 °C for 4 h using a heating rate of 4 °C min^{-1}.

2.2 Powders and pellets characterization

Thermogravimetric analysis (TGA) tests of the powders synthesized at 4 minutes were conducted using a Thermal analyzer **STA-780 Series** Stanton Redcroft in air between room temperature and 1000 °C at a heating rate of 5 °C min^{-1}. The electrical conductivity of the as-prepared cathodes was measured in air by the DC Van der Pauw method in the temperature range between 200 °C and 800 °C. The current and potential were measured with a Keithley 2002 8.5D digital multimeter. 4 golden grids were bonded with golden paste onto the edges of the pellets followed by a sintering process at 950 °C for 2 h by using a heating rate of 5 °C min^{-1}; afterwards, 4 Pt wires were connected to the golden grid.

The thermal expansion coefficient (TEC) was measured with a dilatometer Netzsch DIL 402C in air from 20 °C to 1000 °C (5 °C min^{-1}) **with 1 h at two stationary temperatures of 600** and 800 °C, respectively.

2.3 Cathode contact layer preparation

The half cells for both perovskites were fabricated using YSZ as electrolyte in a cathode-supported cell configuration. An YSZ film of 8-16 μm in thickness was deposited onto the pellets using the simple brush method followed by a sintering process at 1000 °C for 4 h and a heating rate of 5 °C min^{-1}.

2.4 Characterization and performance test

The morphological features of the cathode-electrolyte system were observed by cross-section micrographs using a scanning electron microscopy, Tescan Lyra 3 at 15 kV (50,000x). The specific surface area (S_{BET}), of the half-cell was estimated by N_2 adsorption-desorption porosimetry from 30 to 300 °C. **The instrument employed was Tristar II 3020 from**

Micrometrics Instrument Corporation. Pore size distributions were determined from the isotherms by the BJH method.

For electrochemical performance under different conditions, EIS measurements of the half-cells were characterized using an impedance gain/phase analyzer (Solartron 1260) with two sinusoidal **AC signal amplitudes:** 0.06 and 0.08 V. The measurements were performed at different overpotentials from 0.5 to 1.2 V in the frequency range from 1 MHz to 1 Hz at different range of temperatures from 600 to 800 °C. The data to adjust polarization resistance and specific **impedance were** analyzed with Zview Software.

3. RESULTS AND DISCUSSION

3.1 Pellet characterization

In order to identify the mass loss of the gaseous oxygen, TGA profiles were characterized for the $La_{0.7-x}Pr_xCa_{0.3}MnO_3$ perovskites containing different molar mass of Pr. This technique has been used as a parameter to indicate if the prepared perovskites present oxygen uncoupling property, which in turn suggests that a fast fuel combustion reaction can be reached [35]. **In the thermograms (Figure 1), the first step from room temperature to 115 °C is attributed to the loss of adsorbed moisture in the samples (0.2-3.3 %)**. Subsequent decompositions were observed with a Pr amount of 0.35 and 0.63, whereas sample with Pr =0.52 presents a fairly constant behavior. **The successive steps observed at 115-335 °C and 335-540°C present a mass loss of 1.27-2.91 % and 2.95- 4.26%, for $La_{0.07}Pr_{0.63}Ca_{0.3}MnO_3$ and $La_{0.35}Pr_{0.35}Ca_{0.3}MnO_3$, respectively. These steps are related to the elimination of** CO/**CO_2 adsorbed on the sample surface and/or decomposition of other adsorbed materials (NO_2) [36, 37]. The subsequent weight loss (0.8-2.54%) starts at ~540 °C and ends at ~670 °C; this step has been attributed to the oxygen elimination from the crystalline lattice. The last drop in the mass (0.52-1%) occurring above 670 °C is due to the formation of oxygen vacancies [38-40]. Thus, total mass loss is ~14.31% for $La_{0.35}Pr_{0.35}Ca_{0.3}MnO_3$ perovskites and 7.01% for $La_{0.07}Pr_{0.63}Ca_{0.3}MnO_3$ electrode materials. The mass loss in the last step suggests an adequate behavior for the ORR [41]. The constant weight observed during TGA measurements for samples with molar mass of Pr =0.52 can be explained in term of**

a stable formation of LPCM compound (small changes in the degree of cation ordering) or with low capacity to absorb humidity or CO/CO_2 gases, which is influenced by the surface area or pore volume, necessary to form oxygen vacancies[41, 42].

Figure 2 displays the thermal expansion behavior of the $La_{0.7-x}Pr_xCa_{0.3}MnO_3$ samples in the range from 200 to 1000 °C, it is important to mention that temperatures were kept constant at 600 °C and 800 °C for 1 h to acquire the **thermal expansion coefficient (TEC) values**. For comparison, pellets of YSZ sintered at 1500°C were also evaluated. The plot describes changes of the linear expansion ($\Delta L/L_0$), in the pellet thickness, with the temperature (°C). YSZ displays average TEC values of 9.24×10^{-6} K^{-1} whereas the LPCM perovskite pellets display the following order of TEC values: 12.91×10^{-6} K^{-1} (Pr=0.63)> 10.37×10^{-6} K^{-1} (Pr=0.52)> 7.42×10^{-6} K^{-1} (Pr=0.35). **The TEC values between the cathode material and the electrolyte must be as close as possible to prevent delamination or cracking between the components [43].** These results suggest that **a** high Pr amount in the LPCM enhances the average TEC values in comparison with YSZ; however, the values **are still** in the range previously observed for other manganites-type electrodes**:** $LaMnO_3$ (12.5×10^{-6} K^{-1}), $Pr_{0.7}Ca_{0.3}MnO_3$ (11.9×10^{-6} K^{-1}), $La_{0.8}Ca_{0.2}MnO_3$ (10×10^{-6} K^{-1}), **and** $CaMnO_3$ (17.5×10^{-6} K^{-1}) [44, 45]. **Thus, it is expected that the as-prepared samples will not present adverse effects on the mechanical properties and combustion performance in the SOFC devices.** The increase in the TEC values has been correlated with the increase in the oxygen vacancies in the network through the substitution of ions in the A site [3, 31, 46, 47]. Other additional factor to consider is t**he chemical compatibility and structural stability the electrode material must display, which is essential for ensuring long term performance of the SOFCs [48]. The results of thermal expansion indicate that** the reduction of Mn cations (Mn^{+4}, Mn^{+3} and Mn^{+2}) causes a reduction in the Mn-O bonding strength according to Pauling´s second rule which in turn promotes an increase in the size of the MnO_6 octahedral sites [49-55]. **As a result, the La substitution with this method of synthesis promotes oxygen vacancies into the perovskite lattice without the formation of secondary phases, thus helping the overall SOFC performance.**

3.2 Characterization of the cathode/electrolyte systems

It is well known that most cathodes tend to react with the electrolyte during the manufacturing or **operation at** the sintering temperature, **which is** normally 50- 100 °C higher than the maximum operating temperature of cathode [56]. An analysis of the possible changes in the morphology was performed in selected cathode/electrolyte systems (Pr = 0.52 or 0.63 at 4 min of reaction) by cross-section SEM images **(Figure 3 a-c)**. From **Figure 3a** and **3c**, it is observed a difference in the brightness of the samples separating the electrolyte and LPCM morphologies. From these images, the thickness of the electrolyte was estimated to be 8.51, 15.76 and 15.62 μm for a Pr molar mass of 0.63, 0.52 and 0.35, respectively. This difference in thickness is due to the brush application method used to apply the electrolyte. Nevertheless, this type of application shows a variety of advantages such as a low cost **and ease** of fabrication and it can be applied at laboratory and **industry scale [57-61]. It is seen that all the systems display similar morphology with spaces between the particles with an apparent good coupling between the two materials.** The perovskites are formed by elongated particles in coral reef shape which become larger with reaction time. The spaces between the connections can be correlated with the manganese reduction and the increase of oxygen vacancies. On the contrary, YSZ displays a typical compact semispherical morphology with defined borders between grains and irregular sizes [9, 62].

It has been previously stated that the morphology is dependent of the preparation method, for example, the manganite $Ca_{0.9}Gd_{0.1}MnO$ synthesized by citrate method has shown morphologies with ellipsoid particles concentrated in the grain boundary and intergrains of spherical and polyhedric shapes [29]; whereas $LaMO_3$ perovskites with different elements in the B site (M=Al, Cr, Mn, Fe, Co) synthesized by the microwave-assisted method have shown polyhedric particles of submicron or nanometric size [30]. **Additionally, it has been shown that the morphology is also affected by the temperature, $LaMnO_3$ perovskite sintered at 1300 °C showed a compact and void- free morphology with high density [63].**

BET and BJH isotherms were used to evaluate the surface area and porosity of the LPCM/YSZ systems (Figure 4 a-b). The volume adsorbed **displays low** values (< 1 cm^3 g^{-1} STP) up to the relative pressure reaching values above 0.8. The high quantity absorbed was observed for LPCM/YSZ systems containing 0.63 of Pr. The isotherms display a type II isotherm with H3 type hysteresis (IUPAC classification) which is characteristic of non-porous adsorbent solids or macro-porous systems [64]. Among the as-obtained LPCM/YSZ, the

highest S_{BET} was obtained with Pr=0.63 (27.06 $m^2 g^{-1}$) followed by the composition of Pr=0.35 (21.71 $m^2 g^{-1}$), whereas S_{BET} was considerably lower for that obtained with Pr=0.52 (3.90 $m^2 g^{-1}$). This order was also confirmed by BJH adsorption isotherms with values of 21.92, 17.91 and 0.896 $m^2 g^{-1}$, respectively. The samples that probably display a quasi-spherical shape show the highest surface area, whereas those with irregular morphology **tend** to reduce the BET and BJH surfaces [65]. The surface area, pore volume and pore size improvements contribute to the reaction rate by increasing the active sites via larger exposure of catalysts to the reactants in the three-phase boundary region [66].

Materials that are candidate to be used as cathode in SOFCs require a high performance in oxygen electrochemical reduction. The cathode is one of the critical components but at the interphase with the electrolyte**,** a large ohmic resistance can exist, thus electrical and oxygen anion conductivities were characterized by van der Pauw and EIS**. Figure 5-a** shows the electrical conductivity of as-prepared pellets using 4 minutes of reaction as a **function of temperature (200-800 °C)**. These perovskite-type ceramics **have rarely been reported** and the values of total conductivity vary from 139 to 320 S cm^{-1} between 1000-1300 °C [67-69]. The calculated conductivities were found to be in the range between 5.4 x 10^{-2} and 161.8 x 10^{-2} S cm^{-1} at 800 °C. As expected, the increase in temperature promotes the conductivity in the as-obtained perovskites, which is in agreement with previous characterizations. Next, the measured conductivities were obtained in the following order 161.8 × 10^{-2} (Pr= 0.52) > 23.2 × 10^{-2} (Pr= 0.63) > 5.4 × 10^{-2} (Pr= 0.35) S cm^{-1}. The important differences in the electrical conductivity of the perovskites can be correlated with the reduction in the oxygen vacancies, which depend on the morphology of each sample. Also, inhomogeneous particle size distribution and compactness of the electrode have been reported as the cause of **such difference;** however, porosity is required for LPCM to be used as cathode material. Thus, LPCM/YSZ systems with high surface area and pore volume **(Pr = 0.63 and 0.35),** were clearly expected to display lower electrical conductivity since this property decreases with increasing porosity [70, 71]. Additionally, the temperature-dependent conductivity has been previously established in terms of small polaron hopping model [67, 72-74]. This model is a thermally activated process at lower temperatures and occurs through the transition metal, oxygen, transition metal chain (B-O-B), respectively [37, 75-77]. Pr^{+3} is more stable than Sr^{+2} which is previously reported as dopant in this kind of perovskites. Thus**,** it is expected that the

difference of charge between Pr^{+3} and Ca^{+2}, improves the concentration of oxygen vacancies promoting the oxidation state change of Mn (from +3 to +4) [67, 78].

To corroborate the conductivity mechanism through p-type small polarons, Arrhenius plots were obtained (**Figure 5b**). When carrier concentration remains constant in a temperature range, the Arrhenius plot should be linear [79]. **Thus,** the activation energy (Ea) was obtained by the following equation $ln\sigma = -\frac{E_a}{k}\left(\frac{1}{T}\right) + lnA$; where σ is the conductivity of the material (S cm^{-1}**), A is the pre-exponential factor, Ea** is the activation energy (eV), k is the Boltzmann constant (8.617×10^{-5} eV K^{-1}), **and T is the absolute temperature (K). Ea values for the different perovskites were found to be around 0.129 eV for Pr= 0.52, 0.084 eV for Pr = 0.63 and 0.071 eV for Pr = 0.35.** According to Patra et al [80], a low Ea benefits the jump of electrons. Ea values ca. 0.11 and 0.28 eV have been reported for $Ba_{1-x}Sr_xCo_{0.8}Fe_{0.2}O_{3-\delta}$ perovskites modified with Sr^{+2} in site A at 0.8 and 0.5 molar content. By comparing those values with our systems, the addition of praseodymium **in the microwave irradiation synthesis produces a reduction in the activation energy values since these were found similar or even lower than those reported for perovskites modified with Sr** [77, 81, 82]. The results are also in good agreement with the values reported for an electronic transport model involving electron hopping while the Ea values are comparable or lower than other kind **of perovskites** $(La_{1-x}Sr_x)_{0.85}MnO_3$ synthesized from commercial powders (0.132 eV) [68, 83]**.**

The ionic conductivity in dependence of the temperature (600-800°C) was evaluated by EIS technique. The experiments were performed at different applied overpotentials (0.5-1.2 V) and two different sinusoidal AC voltage perturbation signals (0.06, 0.08 V_{rms}) over a frequency range from 10^0 to 10^6 Hz in static air. The electrochemical measurements were performed for all as-obtained specimens, but only representative LPCM/YSZ systems that presented the low charge transfer resistance with a Pr molar mass of 0.63 and 0.35, are presented in Figures 6 a-d and 7 a-d (see also supplementary information). EIS spectra for $La_{0.07}Pr_{0.63}Ca_{0.3}MnO_3$ systems show that an increase in the sinusoidal voltage perturbation tends to increase the polarization resistance (Rp) (Figure 6 a-d). **As it is known, small voltage perturbation (5 or 10 mV) are applied in the majority of experiments, however, the as-prepared system behaves with nonlinear effects, especially at operating temperatures of 600 °C. These effects are noticeable at intermediate-low**

frequency regions, and thus, it is considered that the impedance is a function of the applied perturbation amplitude. Some investigations comment that application of a large amplitude can conduce to some errors in quantitative estimation, but the mechanism of ionic conductivity is the same. In this case, the nonlinear effects and the application of high sinusoidal voltage perturbation did not cause an important data dispersion, suggesting an adequate amplitude to evaluate the LPCM/YSZ systems. This assumption can be confirmed with an increase in the temperature and with the reduction of the nonlinear effects. The EIS spectra are quite comparable [84, 85]. A similar trend, where the Rp increases with an augment of the perturbation amplitudes at low temperatures (600 °C), was observed for $La_{0.35}Pr_{0.35}Ca_{0.3}MnO_3$ systems (Figure 7a-d). It is again obtained an important similarity in EIS spectra at operating temperatures of 700 and 800 °C[84, 85]. On the other hand, the increase in the cathodic overpotential enlarged the ionic conductivity, but in some samples no clear trend can be anticipated.

Then, EIS measurements confirm that the electrode is stable due to no change in the ionic conductivity mechanism with the applied temperature and that a high Pr concentration causes a positive effect in the polarization resistance of LPCM/YSZ systems promoting oxygen vacancies that help to increase the ionic conductivity.

It is also evident that all the samples display **two main contributions at high and low frequencies. These time constants are related to the reduction of molecular oxygen to oxygen ions and/or charge transfer resistance, as well as the adsorption/gas diffusion inside the porous cathode[37]**. The shape of obtained EIS spectra has been previously reported indicating that molecular oxygen diffusion along the gas-phase boundary layer acts as the rate-determining step of the reduction reaction[86].

EIS spectra were fitted by typical equivalent circuits and consist of $R_1(R_{HF}CPE_{HF})(R_{LF}CPE_{LF})$, Figure 8a [18]. R_1 relates to the ohmic resistance in the electrolyte, R_{HF} is associated to the oxygen vacancy exchange at the electrode/electrolyte interphase $O_2 \rightarrow 2O^{2-}$, R_{LF} corresponds to the adsorption and diffusion of oxygen at the surface of cathode electrode [87, 88]. The CPE_{HF} and CPE_{LF} simulate an imperfect capacitor in the charge transfer process in the electrolyte/electrode interphase and polarization resistance at low frequencies, respectively. Considering that $Z_{CPE} = {}^{1}/_{(Y_o(j\,\omega)^n)}$, ω is the angular frequency, Y_o is the relative capacitance and $Y_o = C^n(R_1^{-1} + R_{HF\ or\ LF}^{-1})^{1-n}$; n is the CPE

exponent (the value of n is in the range from 0-1). In the **Figures 6 and 7,** the continuous lines **represent** the best fit, which was considered with a $\chi^2 \leq 10^{-3}$. The numerical data of fitted results are shown in **Table 1** for samples with the best electrochemical performance **with an amount of Pr** = 0.35 and 0.63. In addition, this table shows the ionic conductivity computed from the classical formula $\sigma = \frac{L}{(R)(S)}$, where σ is the perovskite conductivity (S cm^{-1}), S is the surface area of the material, **calculated with the circle area equation $A = \pi r^2$ and BET analysis**, R corresponds to the material resistance (Ω) and L is the pellet thickness (0.15 cm). From **Table 1**, it is seen that R_1 values were found in the range of 0.26 × 10^{-3} to 0.97 × 10^{-3} Ω cm^2 for **$La_{0.07}Pr_{0.63}Ca_{0.3}MnO_3$ systems** and 1.27 × 10^{-3}- 2.53 × 10^{-3} Ω cm^2 **for samples with Pr amount of 0.35 molar mass.** The small differences can be ascribed to insignificant changes in the adhesion strength due to the variations in the thermal expansion coefficient in dependence of the Pr amount [37, 87]. Comparing the R_{HF} and R_{LF} values, it is clearly seen, in the temperature range evaluated, that R_{HF} values were very large which has been correlated with the changes between electric and ionic resistance; i.e, high R_{HF} values suggest that the cathode surface is highly dependent of electrical conductivity at temperatures above 600 °C. Typical trend of decreasing Rp values in the samples with temperature confirms the thermal activation on the **LPCM/YSZ systems.**

On the other hand, the relative capacitance in samples with 0.63 molar mass Pr tends to decrease with the temperature from 3.17-2.98 × 10^{-7} ($\Omega^{-1}cm^{-2}s^n$) in the case of Y_{oHF} and 8.51-0.22 × 10^{-3} ($\Omega^{-1}cm^{-2}s^n$) Y_{oLF}. **Samples with a molar mass of Pr = 0.35 (maintaining a constant overpotential 1.2 V) did not show a clear trend in the relative capacitances. At** Y_{oHF} the relative capacitance values increase with temperature from 3.18-3.82 × 10^{-7} ($\Omega^{-1}cm^{-2}s^n$) whereas at low frequencies **the relative capacitances (Y_{oLF}) is reduced** from 95.66-3.08 × 10^{-3} ($\Omega^{-1}cm^{-2}s^n$). Then, the operating temperature causes an **increase in the** oxygen vacancies concentration modifying the pseudo-capacitance in the cathode/electrolyte interphase (high frequency regions), but it **is highly** dependent of the Pr content. **The numerical values confirm that the kinetics of oxygen reduction reaction enhanced with the temperature and was more effective with low applied sinusoidal voltage perturbation.**

From the $R_p = (R_1+R_{HF}+R_{LF})$ values, the lowest polarization resistance of 5.86 Ω cm^2 was observed for $La_{0.07}Pr_{0.63}Ca_{0.3}MnO_3$ systems (η=0.9 V, 800 °C and 0.06 V of amplitude). At **800 °C, the other** two samples display similar Rp values 6.39 Ω cm^2 (η= 1.2 V and 0.08 V of

amplitude) and 6.54 Ω cm^2 (η= 0.6 V and 0.08 V of amplitude). In the case of samples with a Pr molar mass of 0.**35 and η=1.2 V, the lowest values were also observed at 800 °C, i.e. from** 14.19 Ω cm^2 (η= 1.2 V and 0.06 V of amplitude) to 17.30 Ω cm^2 (η= 1.2 V and 0.08 V of amplitude). **The results suggest that a quantity of 0.63 molar mass of Pr is more adequate to promote an interaction in the interphase as well as improvement in the catalytic activity, although samples with 0.35 Pr also present an adequate electroactivity for the ORR.**

The electrical conductivity of these samples is also shown in **Table 1**. The high σ was again observed for samples with a composition of 0.63 Pr at 800 °C following the order described above. **In the best case, the conductivity value was 19.97 × 10^{-3} S cm^{-1} (η= 0.9 V, 800 °C and 0.06 V of amplitude). The activation energy (**E_a**) for this system was** 0.8× 10^{-3} eV, which **was determined from the Arrhenius equation at the temperature range from 600 to 800 °C. The high conductivity in the sample with an amount of 0.35 Pr was about 8.24 × 10^{-3} eV, which was observed for samples at η= 1.2 V, 800 °C and 0.06 V of amplitude .**

It can be seen that **by comparing the** van der Pauw and EIS results**, both techniques,** display a similar trend in the electrical conductivity, although, they show a mismatch of an order in magnitude. The differences can be explained in terms of the techniques **by** themselves. Although both can be used for proper determination of electrical conductivity, EIS is **an AC** technique that is evaluated in a frequency range **of 10^0-10^6 Hz an**d that was normalized with the BET area; whereas van der Pauw is a **DC method** that only considers the geometric area.

In such conditions, two types of ionic conduction mechanism are possible: the first pathway **can be** explained in terms of the oxygen vacancies formed during the synthesis (atomic level). Pr substituting La in A-site increases the concentration of the oxygen vacancies **through the compensation of perovskite stoichiometry, which in turn compensates the $Mn^{3+} \rightarrow Mn^{4+} + e^-$ oxidation in terms of the Schottky intrinsic disorder [20, 89, 90];**

$$6Mn_{Mn}^{x} + \frac{3}{2}O_2 \underset{\leftarrow}{\rightarrow} 6Mn_{Mn}^{\cdot} + 2O_O^x + V_{La}''' + V_{Mn}''' \quad (1)$$

In this case, the stability of adsorbed **molecules** and the dissociation of the oxygen species depend on the orientation and defects in the perovskite. **Thus, the oxygen vacancies on the surface improve the dissociation rate of the oxygen species due to the reduction of the E_a provoked by the substitution of La for Pr in the A-site [91].**

$$La_{0.07}Pr_{0.63}Ca_{0.3}MnO_3V_{(s)} + O_{2(g)} \xrightarrow{adsorption} O_2 - La_{0.07}Pr_{0.63}Ca_{0.3}MnO_3V_{(s)}$$
$$\xrightarrow{dissociation} 2O - La_{0.07}Pr_{0.63}Ca_{0.3}MnO_3V_{(s)} \xrightarrow{incorporation} O - La_{0.07}Pr_{0.63}Ca_{0.3}MnO_3O_{(s)} \quad (2)$$

or

$$La_{0.07}Pr_{0.63}Ca_{0.3}MnO_3V + O_{2(g)} \xrightarrow{incorporation} O - La_{0.07}Pr_{0.63}Ca_{0.3}MnO_3O_{(s)} \quad (3)$$

The other possible pathway occurs at bulk scale and is correlated with the porosity of the system. The gas/solid interphase and the bulk transport phenomenon are affected by the structural parameters, such as porosity and surface area. In the ORR, the electrons are attracted by the molecular oxygen to produce the current that passes through the electrode [**Error! Bookmark not defined.**]. According to previous results, **it is believed that both mechanisms are present in the LPCM/YSZ systems**. **A schematic representation of the combination pathway is presented in Figure 8b. The scheme represents a porous cathode with 0.15 cm of thickness where oxygen dissociation is stimulated through oxygen vacancies produced by Praseodymium-substituted lanthanum, which in turn favored the gas diffusion and charge transfer resistance in the LPCM/YSZ interphase.**

It is shown that the triple phase boundaries (TPB) exist between the intersection of gas with the LPCM cathode and the YSZ electrolyte. It was also necessary to consider the connectivity of the gaseous phase **between electrode and electrolyte, where oxygen molecule diffuses through the open pores of the electrode and reduces into TPB to O^{2-}.** The conductive path of the electrons in the interface occurs through the LPCM connected to a current source outside the interface. The oxide ions formed by ORR are incorporated into the electrolyte (YSZ) and thereafter, they are ready to diffuse toward **the** anode under the influence of chemical potential gradient. **The available active sites (i.e., oxygen vacancies) significantly improved the ORR kinetics and in this case, it was at temperatures below 1000 °C.**

Based on the results of the structure and morphology of the LPCM/YSZ systems and the proposed scheme, it can be concluded that the Pr0.63/YSZ **systems presented the higher oxygen vacancies and better TPB formation compared to the Pr0.35/YSZ electrodes, however, a fraction of 0.35 Pr can also act as adequate electrode material for ORR.**

4. CONCLUSSIONS

$La_{0.7-x}Pr_xCa_{0.3}MnO_3$ perovskite pellets with different stoichiometry (x=0.35, 0.52 and 0.63) previously obtained through the microwave-assisted method **for** 4 minutes were examined as potential cathode material for SOFCs applications from 600 to 800 °C.

The TGA results **revealed the presence of uncoupling oxygen in the perovskites doped with** 0.35 and 0.63 of Pr, **favoring** the promotion of the oxygen vacancies from **650 °C which in turn** favors the fuel combustion.

The TEC **values** of **these** perovskites were **found to be** closer to the value of YSZ **demonstrating a good thermal compatibility with the electrolyte under air atmosphere as well as adequate stability to avoid cracking and failing during fabrication and operation in** cathode applications**, especially the samples doped with** 0.63 of Pr.

The morphologies of the pellets exhibited elongated and coral reef shape particles, which indicated a good coupling with the electrolyte. **A correlation of the morphology with the surface area was found, in that the regular quasi-spherical shape showed the highest value in BET and BJH whereas the irregular ones reduced them.**

The calculated conductivities by van der Pauw method were found in the order of 10^{-2} S cm^{-1} and the differences between samples can be correlated with the availability of oxygen vacancies. Electrodes with a Pr amount of 0.35 presented **Ea value of 0.071 eV**, slightly lower than materials with an amount of Pr =0.65 (0.084 eV).

On the contrary, EIS characterization at high temperature (600 - 800 °C) showed that electrode materials with a Pr molar mass of 0.63 LPCM/YSZ (η= 0.9 V, 800 °C and 0.06 V of amplitude) display about twice the values of ionic conductivity in comparison with LPCM/YSZ systems with an amount of Pr= 0.35 (η= 1.2 V, 800 °C and 0.06 V of amplitude).

From the results of the overall characterizations, it was found that the oxygen vacancies were better promoted with a molar mass of Pr= 0.65 in the $La_{0.7-x}Pr_xCa_{0.3}MnO_3$ perovskite, which facilitate a fast oxygen dissociation with an improvement in the ionic conductivity, although samples with a Pr= 0.35 can also act efficiently in the ORR. The synthesis of perovskites by microwave irradiation method can modulate the morphology and promote TPB connectivity. Thus, findings demonstrate that $La_{0.7-x}Pr_xCa_{0.3}MnO_3$

perovskites can be promising electrode materials to be used as potential candidate for cathode in SOFCs applications.

Author contributions

Authors A.C. Ferrel- Alvarez, M.A. Domínguez-Crespo, H. Cong, A.M. Torres- Huerta, D. Palma- Ramírez and J. T. S. Irvine all participate in formal analyses, data curation, investigation and methodology. A.C. Ferrel- Alvarez and M.A. Domínguez-Crespo were responsible for writing-review & edition. M.A. Domínguez-Crespo, H. Cong, A. M. Torres-Huerta and J. T. S. Irvine were also responsible for science conceptualization, resources, supervision and **funding acquisition**.

Declaration of Competing Interest

The authors declare that they have no known competing financial interests or personal relationships that could have appeared to influence the work reported in this paper.

ACKNOWLEDGEMENTS

Atzin Ferrel is grateful for her grants from CONACYT and SIP- IPN. The authors also appreciate the financial support provided by the Consejo Nacional de Ciencia y Tecnología (CONACYT), México, Comisión de Operación y Fomento de Actividades Académicas del IPN (COFAA), México and Secretaría de Investigación y Posgrado (SIP) of the Instituto Politécnico Nacional (IPN) México through the CB2015-252181, 20201278, 20201279, 20201280, 20202443 and 20200909 projects as well as the SNI-CONACyT.

REFERENCES

[1] X. Peng, Y. Tian, Y. Liu, W. Wang, c. Jing, J. Li, B. Chi, J. Pu, J. Li, A double perovskite decorated carbon-tolerant redox electrode for symmetrical SOFC, International Journal of Hydrogen Energy, 45 (2020) 14461-14469.

[2] M.K. Rath, K.-T. Lee, Investigation of aliovalent transition metal doped La0.7Ca0.3Cr0.8X0.2O3−δ (X=Ti, Mn, Fe, Co, and Ni) as electrode materials for symmetric solid oxide fuel cells, Ceramics International, 41 (2015) 10878-10890.

[3] W. Li, C.Y. Xiong, L.C. Jia, J. Pu, B. Chi, X. Chen, J.W. Schwank, J. Li, Strontium-doped samarium manganite as cathode materials for oxygen reduction reaction in solid oxide fuel cells, Journal of Power Sources, 284 (2015) 272-278.

[4] A.B. Stambouli, E. Traversa, Solid oxide fuel cells (SOFCs): a review of an environmentally clean and efficient source of energy, Renewable and Sustainable Energy Reviews, 6 (2002) 433-455.
[5] L.S. Mahmud, A. Muchtar, M.R. Somalu, Challenges in fabricating planar solid oxide fuel cells: A review, Renewable and Sustainable Energy Reviews, 72 (2017) 105-116.
[6] S. Sydyknazar, V. Cascos, M.T. Fernández-Díaz, J.A. Alonso, Design, synthesis and performance of Ba-doped derivatives of SrMo0.9Fe0.1O3-δ perovskite as anode materials in SOFCs, Journal of Materiomics, 5 (2019) 280-285.
[7] M. Sharifzadeh, N. Shah, Chapter 6 - Synthesis, integration, and intensification of solid oxide fuel cell systems: process systems engineering perspective, in: M. Sharifzadeh (Ed.) Design and Operation of Solid Oxide Fuel Cells, Academic Press, 2020, pp. 185-215.
[8] A.F. Al-Attar, S.B.H. Farid, F.A. Hashim, M.J. Eshraghi, Comparison in Physical and Mechanical Properties between Doped and Non-Doped Y-TZP Electrolyte for HT-SOFC, Energy Procedia, 157 (2019) 1285-1291.
[9] J. Zhang, C. Lenser, N.H. Menzler, O. Guillon, Comparison of solid oxide fuel cell (SOFC) electrolyte materials for operation at 500 °C, Solid State Ionics, 344 (2020) 115138.
[10] C.C. Wang, S. Darvish, K. Chen, B. Hou, Q. Zhang, Z. Tan, Y. Zhong, S.P. Jiang, Combined Cr and S poisoning of La0.8Sr0.2MnO3-δ (LSM) cathode of solid oxide fuel cells, Electrochimica Acta, 312 (2019) 202-212.
[11] S.S.C.C.a.L. Zhang, Perovskites and Related Mixed Oxides for SOFC Applications, in: V.I.P. Pascal Granger, Serge Kaliaguine, Wilfrid Prellier (Ed.) Perovskites and Related Mixed Oxides: Concepts and Applications, John Wyley & Sons, Inc., 2016, pp. 863-876.
[12] T. Horita, H. Kishimoto, K. Yamaji, M.E. Brito, Y. Xiong, H. Yokokawa, Y. Hori, I. Miyachi, Effects of impurities on the degradation and long-term stability for solid oxide fuel cells, Journal of Power Sources, 193 (2009) 194-198.
[13] J.A. Schuler, H. Yokokawa, C.F. Calderone, Q. Jeangros, Z. Wuillemin, A. Hessler-Wyser, J. Van herle, Combined Cr and S poisoning in solid oxide fuel cell cathodes, Journal of Power Sources, 201 (2012) 112-120.
[14] N.Q. Minh, Solid oxide fuel cell technology—features and applications, Solid State Ionics, 174 (2004) 271-277.
[15] Y. Chen, Y. Fan, S. Lee, G. Hackett, H. Abernathy, K. Gerdes, X. Song, Interface and grain boundary degradation in LSM-YSZ composite Solid Oxide Fuel Cell cathodes operated in humidified air, Journal of Power Sources, 438 (2019) 227043.
[16] Y. Niu, W. Lv, D. Chen, J. Han, W. He, A model study on correlation between microstructure-gas diffusion and Cr deposition in porous LSM/YSZ cathodes of solid oxide fuel cells, International Journal of Hydrogen Energy, 44 (2019) 18319-18329.
[17] D. Garcés, A.L. Soldati, H. Troiani, A. Montenegro-Hernández, A. Caneiro, L.V. Mogni, La/Ba-based cobaltites as IT-SOFC cathodes: a discussion about the effect of crystal structure and microstructure on the O2-reduction reaction, Electrochimica Acta, 215 (2016) 637-646.
[18] W. Guo, R. Guo, L. Liu, G. Cai, C. Zhang, C. Wu, Z. Liu, H. Jiang, Thermal and electrochemical properties of layered perovskite PrBaCo2−xMnxO5+δ (x = 0.1, 0.2 and 0.3) cathode materials for intermediate temperature solid oxide fuel cells, International Journal of Hydrogen Energy, 40 (2015) 12457-12465.
[19] S.B. Adler, Factors Governing Oxygen Reduction in Solid Oxide Fuel Cell Cathodes, Chemical Reviews, 104 (2004) 4791-4844.
[20] N. Mahato, A. Banerjee, A. Gupta, S. Omar, K. Balani, Progress in material selection for solid oxide fuel cell technology: A review, Progress in Materials Science, 72 (2015) 141-337.
[21] D. Ding, X. Li, S.Y. Lai, K. Gerdes, M. Liu, Enhancing SOFC cathode performance by surface modification through infiltration, Energy & Environmental Science, 7 (2014) 552-575.

[22] S.P. Jiang, Development of lanthanum strontium manganite perovskite cathode materials of solid oxide fuel cells: a review, Journal of Materials Science, 43 (2008) 6799-6833.
[23] J.H. Kim, J.T.S. Irvine, Characterization of layered perovskite oxides NdBa1−xSrxCo2O5+δ (x = 0 and 0.5) as cathode materials for IT-SOFC, International Journal of Hydrogen Energy, 37 (2012) 5920-5929.
[24] J.W. Fergus, Materials challenges for solid-oxide fuel cells, JOM, 59 (2007) 56-62.
[25] M. Park, H.Y. Jung, J.Y. Kim, H. Kim, K.J. Yoon, J.-W. Son, J.-H. Lee, B.-K. Kim, H.-W. Lee, Effects of mixing state of composite powders on sintering behavior of cathode for solid oxide fuel cells, Ceramics International, 43 (2017) 11642-11647.
[26] A.J. McEvoy, Thin SOFC electrolytes and their interfaces–: A near-term research strategy, Solid State Ionics, 132 (2000) 159-165.
[27] C. Sun, R. Hui, J. Roller, Cathode materials for solid oxide fuel cells: a review, Journal of Solid State Electrochemistry, 14 (2010) 1125-1144.
[28] M. Balaguer, V.B. Vert, L. Navarrete, J.M. Serra, SOFC composite cathodes based on LSM and co-doped cerias (Ce0.8Gd0.1X0.1O2–δ, X = Gd, Cr, Mg, Bi, Ce), Journal of Power Sources, 223 (2013) 214-220.
[29] M. Rosić, L. Kljaljević, D. Jordanov, M. Stoiljković, V. Kusigerski, V. Spasojević, B. Matović, Effects of sintering on the structural, microstructural and magnetic properties of nanoparticle manganite Ca1−xGdxMnO3 (x=0.05, 0.1, 0.15, 0.2), Ceramics International, 41 (2015) 14964-14972.
[30] J. Prado-Gonjal, Á.M. Arévalo-López, E. Morán, Microwave-assisted synthesis: A fast and efficient route to produce LaMO3 (M=Al, Cr, Mn, Fe, Co) perovskite materials, Materials Research Bulletin, 46 (2011) 222-230.
[31] A. Mahata, P. Datta, R.N. Basu, Synthesis and characterization of Ca doped LaMnO3 as potential anode material for solid oxide electrolysis cells, Ceramics International, 43 (2017) 433-438.
[32] Y. Takeda, Y. Sakaki, T. Ichikawa, N. Imanishi, O. Yamamoto, M. Mori, N. Mori, T. Abe, Stability of La1−xAxMnO3−z (A=Ca, Sr) as cathode materials for solid oxide fuel cells, Solid State Ionics, 72 (1994) 257-264.
[33] J. Zhao, C. Li, L. Kong, X. Wu, Y. Ma, Synthesis and characterization of calcium and manganese-doped rare earth oxide La1-xCaxFe0.9Mn0.1O3-δ for cathode material in IT-SOFC, Journal of Rare Earths, 29 (2011) 1066-1069.
[34] A.C. Ferrel-Álvarez, M.A. Domínguez-Crespo, H. Cong, A.M. Torres-Huerta, S.B. Brachetti-Sibaja, W. De La Cruz, Synthesis and surface characterization of the La0.7-xPrxCa0.3MnO3 (LPCM) perovskite by a non-conventional microwave irradiation method, Journal of Alloys and Compounds, 735 (2018) 1750-1758.
[35] R.L.B.A. Medeiros, V.R.M. Melo, D.M.A. Melo, H.P. Macedo, G.T. Moure, I. Adánez-Rubio, M.A.F. Melo, J. Adánez, Double perovskite (La2-xCa-Bax)NiO4 oxygen carriers for chemical looping reforming applications, International Journal of Hydrogen Energy, 45 (2020) 1681-1696.
[36] D.R. Sahu, D.K. Mishra, S.H. Hung, P. Pramanik, B.K. Roul, La0.67Ca0.33MnO3 thin films on Si (100) by DC magnetron sputtering technique using nanosized powder compacted target, Materials Research Bulletin, 42 (2007) 1119-1127.
[37] T. Ghorbani-Moghadam, A. Kompany, M.M. Bagheri-Mohagheghi, M.E. Abrishami, High temperature electrical conductivity and electrochemical investigation of La2-xSrxCoO4 nanoparticles for IT-SOFC cathode, Ceramics International, 44 (2018) 21238-21248.
[38] F. Jin, H. Xu, W. Long, Y. Shen, T. He, Characterization and evaluation of double perovskites LnBaCoFeO5+δ (Ln = Pr and Nd) as intermediate-temperature solid oxide fuel cell cathodes, Journal of Power Sources, 243 (2013) 10-18.

[39] V. Cascos, M.T. Fernández-Díaz, J.A. Alonso, Structural and electrical characterization of the novel SrCo1-xTixO3–δ (x = 0.05, 0.1 and 0.15) perovskites: Evaluation as cathode materials in solid oxide fuel cells, Renewable Energy, 133 (2019) 205-215.
[40] L.M. Kolchina, N.V. Lyskov, P.P. Pestrikov, S.Y. Istomin, G.N. Mazo, E.V. Antipov, Evaluation of La1.8−xPrxSr0.2CuO4−δ oxides as cathode materials for IT-SOFCs, Materials Chemistry and Physics, 165 (2015) 91-96.
[41] M.V. Sandoval, S. Durán, A. Prada, C. Pirovano, O. Gardoll, P. Roussel, G.H. Gauthier, Synthesis and preliminary study of NdxAE2-xMnO4±δ (AE: Ca, Sr) for symmetrical SOFC electrodes, Solid State Ionics, 317 (2018) 194-200.
[42] R. Li, F. Jin, Y. Zhang, B. Niu, J. Liu, T. He, Performance and optimization of perovskite-type La1·4Ca0·6CoMnO5+δ cathode for intermediate-temperature solid oxide fuel cells, International Journal of Hydrogen Energy, 44 (2019) 8467-8478.
[43] Y. Ling, X. Lu, J. Niu, H. Chen, Y. Ding, X. Ou, L. Zhao, Antimony doped barium strontium ferrite perovskites as novel cathodes for intermediate-temperature solid oxide fuel cells, Journal of Alloys and Compounds, 666 (2016) 23-29.
[44] S. Jiang, Development of Lanthanum Strontium Manganite Perovskite Cathode Materials of Solid Oxide Fuel Cells: A Review, Journal of Materials Science, 43 (2008) 6799-6833.
[45] T. Kawada, T. Horita, 6 - Cathodes, in: K. Kendall, M. Kendall (Eds.) High-Temperature Solid Oxide Fuel Cells for the 21st Century (Second Edition), Academic Press, Boston, 2016, pp. 161-193.
[46] G.C. Kostogloudis, N. Vasilakos, C. Ftikos, Preparation and characterization of Pr1-xSrxMnO3 ± δ (x = 0, 0.15, 0.3, 0.4, 0.5) as a potential SOFC cathode material operating at intermediate temperatures (500–700 °C), Journal of the European Ceramic Society, 17 (1997) 1513-1521.
[47] Y. Sakaki, Y. Takeda, A. Kato, N. Imanishi, O. Yamamoto, M. Hattori, M. Iio, Y. Esaki, Ln1−xSrxMnO3 (Ln=Pr, Nd, Sm and Gd) as the cathode material for solid oxide fuel cells, Solid State Ionics, 118 (1999) 187-194.
[48] J.H. Zhu, H. Ghezel-Ayagh, Cathode-side electrical contact and contact materials for solid oxide fuel cell stacking: A review, International Journal of Hydrogen Energy, 42 (2017) 24278-24300.
[49] J.J. Alvarado Flores, Análisis de la estructura perovskita LaxSr1-xCryMn1-yO3-δ con potencial aplicación como ánodo para celdas de combustible de óxido sólido, Boletín de la Sociedad Española de Cerámica y Vidrio, 56 (2017) 73-82.
[50] K.J. Yoon, C.N. Cramer, J.W. Stevenson, O.A. Marina, Improvement of Sintering, Thermal Behavior, and Electrical Properties of Calcium- and Transition Metal-Doped Yttrium Chromite, Electrochemical and Solid-State Letters, 13 (2010) B101-B105.
[51] Y. Tsuru, M. Shimazu, M. Shiono, M. Morinaga, Evaluation of Linear Thermal Expansion Coefficients of Perovskite Oxides UsingAb-initioMolecular Dynamics with Small Cell Sizes for Materials Design, Japanese Journal of Applied Physics, 49 (2010) 045701.
[52] S. Taniguchi, M. Aniya, Relationship Between Thermal Expansion, Ionic Conduction and Ionicity in Perovskite-Type Oxides, Integrated Ferroelectrics, 115 (2010) 18-24.
[53] B.A. Boukamp, The amazing perovskite anode, Nature Materials, 2 (2003) 294-296.
[54] V.V. Kharton, E.V. Tsipis, I.P. Marozau, A.P. Viskup, J.R. Frade, J.T.S. Irvine, Mixed conductivity and electrochemical behavior of (La0.75Sr0.25)0.95Cr0.5Mn0.5O3−δ, Solid State Ionics, 178 (2007) 101-113.
[55] H. Ullmann, N. Trofimenko, F. Tietz, D. Stöver, A. Ahmad-Khanlou, Correlation between thermal expansion and oxide ion transport in mixed conducting perovskite-type oxides for SOFC cathodes, Solid State Ionics, 138 (2000) 79-90.
[56] M. Jafari, H. Salamati, M. Zhiani, E. Shahsavari, Enhancement of an IT-SOFC cathode by introducing YSZ: Electrical and electrochemical properties of La0.6Ca0.4Fe0.8Ni0.2O3-δ-YSZ composites, International Journal of Hydrogen Energy, 44 (2019) 1953-1966.

[57] R. Liu, C. Zhao, J. Li, S. Wang, Z. Wen, T. Wen, Testing of a cathode fabricated by painting with a brush pen for anode-supported tubular solid oxide fuel cells, Journal of Power Sources, 195 (2010) 541-545.
[58] F.C. Antunes, C.A. Goulart, M.R.B. Andreeta, D.P.F. de Souza, YSZ/Al2O3 multilayer thick films deposited by spin coating using ceramic suspensions on Al2O3 polycrystalline substrate, Materials Science and Engineering: B, 228 (2018) 60-66.
[59] C. Torres-Garibay, D. Kovar, Perovskite-related intergrowth cathode materials with thin YSZ electrolytes for intermediate temperature solid oxide fuel cells, Journal of Power Sources, 192 (2009) 396-399.
[60] L. Zhang, S. Li, T. Xia, L. Sun, L. Huo, H. Zhao, Co-deficient PrBaCo2−xO6−δ perovskites as cathode materials for intermediate-temperature solid oxide fuel cells: Enhanced electrochemical performance and oxygen reduction kinetics, International Journal of Hydrogen Energy, 43 (2018) 3761-3775.
[61] Y. Yang, Y. Chen, D. Tian, X. Lu, Y. Ding, W. Yu, B. Lin, A new A-site excessive strategy to improve performance of layered perovskite cathode for intermediate-temperature solid oxide fuel cells, Electrochimica Acta, 231 (2017) 686-693.
[62] V. Sadykov, N. Mezentseva, V. Usoltsev, E. Sadovskaya, A. Ishchenko, S. Pavlova, Y. Bespalko, T. Kharlamova, E. Zevak, A. Salanov, T. Krieger, V. Belyaev, O. Bobrenok, N. Uvarov, Y. Okhlupin, O. Smorygo, A. Smirnova, P. Singh, A. Vlasov, M. Korobeynikov, A. Bryazgin, P. Kalinin, A. Arzhannikov, Solid oxide fuel cell composite cathodes based on perovskite and fluorite structures, Journal of Power Sources, 196 (2011) 7104-7109.
[63] A. Galal, N.F. Atta, S.M. Ali, Investigation of the catalytic activity of LaBO3 (B=Ni, Co, Fe or Mn) prepared by the microwave-assisted method for hydrogen evolution in acidic medium, Electrochimica Acta, 56 (2011) 5722-5730.
[64] K.S.W. Sing, D.H. Everett, R.A.W. Haul, L. Moscou, R.A. Pierotti, J. Rouquerol, T. Siemieniewska, Reporting Physisorption Data for Gas Solid Systems with Special Reference to the Determination of Surface-Area and Porosity (Recommendations 1984), Pure Appl Chem, 57 (1985) 603-619.
[65] K. Sakthipandi, V. Rajendran, Metal insulator transition of bulk and nanocrystalline La1−xCaxMnO3 perovskite manganite materials through in-situ ultrasonic measurements, Materials Characterization, 77 (2013) 70-80.
[66] M. Malinowski, A. Iwan, A. Hreniak, I. Tazbir, An anode catalyst support for polymer electrolyte membrane fuel cells: application of organically modified titanium and silicon dioxide, RSC Advances, 9 (2019) 24428-24439.
[67] A. Hammouche, E.J.L. Schouler, M. Henault, Electrical and thermal properties of Sr-doped lanthanum manganites, Solid State Ionics, 28-30 (1988) 1205-1207.
[68] C.N. Chervin, B.J. Clapsaddle, H.W. Chiu, A.E. Gash, J.H. Satcher, S.M. Kauzlarich, A Non-Alkoxide Sol−Gel Method for the Preparation of Homogeneous Nanocrystalline Powders of La0.85Sr0.15MnO3, Chemistry of Materials, 18 (2006) 1928-1937.
[69] J. Richter, P. Holtappels, T. Graule, T. Nakamura, L.J. Gauckler, Materials design for perovskite SOFC cathodes, Monatshefte für Chemie - Chemical Monthly, 140 (2009) 985-999.
[70] S. Presto, P. Kumar, S. Varma, M. Viviani, P. Singh, Electrical conductivity of NiMo–based double perovskites under SOFC anodic conditions, International Journal of Hydrogen Energy, 43 (2018) 4528-4533.
[71] N.Q. Minh, Ceramic Fuel Cells, Journal of the American Ceramic Society, 76 (1993) 563-588.
[72] J.H. Kim, A. Manthiram, LnBaCo2O5 + δ Oxides as Cathodes for Intermediate-Temperature Solid Oxide Fuel Cells, Journal of The Electrochemical Society, 155 (2008) B385-B390.
[73] Y.N. Kim, J.H. Kim, A. Manthiram, Effect of Fe substitution on the structure and properties of LnBaCo2−xFexO5+δ (Ln=Nd and Gd) cathodes, Journal of Power Sources, 195 (2010) 6411-6419.

[74] Q. Zhou, F. Wang, Y. Shen, T. He, Performances of LnBaCo2O5+x–Ce0.8Sm0.2O1.9 composite cathodes for intermediate-temperature solid oxide fuel cells, Journal of Power Sources, 195 (2010) 2174-2181.
[75] H. Fröhlich, Electrons in lattice fields, Advances in Physics, 3 (1954) 325-361.
[76] P. Zhang, G. Guan, D.S. Khaerudini, X. Hao, C. Xue, M. Han, Y. Kasai, A. Abudula, B-site Mo-doped perovskite Pr0.4Sr0.6 (Co0.2Fe0.8)1−xMoxO3−σ (x = 0, 0.05, 0.1 and 0.2) as electrode for symmetrical solid oxide fuel cell, Journal of Power Sources, 276 (2015) 347-356.
[77] P. Kaur, K. Singh, Review of perovskite-structure related cathode materials for solid oxide fuel cells, Ceramics International, (2019).
[78] P. Matheswaran, M. Rajasekhar, A. Subramania, Assisted combustion synthesis and characterization of Pr0.6Sr0.4MnO3±δ nano crystalline powder as cathode material for IT-SOFC, Ceramics International, 43 (2017) 988-991.
[79] Z.S. Talaei, H. Salamati, A. Pakzad, Fabrication and investigation of electrochemical characterization of Ba based cathodes, International Journal of Hydrogen Energy, 35 (2010) 9401-9404.
[80] H. Patra, S.K. Rout, S.K. Pratihar, S. Bhattacharya, Thermal, electrical and electrochemical characteristics of Ba1−xSrxCo0.8Fe0.2O3−δ cathode material for intermediate temperature solid oxide fuel cells, International Journal of Hydrogen Energy, 36 (2011) 11904-11913.
[81] R.E.A. Ngida, M.F. Zawrah, R.M. Khattab, E. Heikal, Hydrothermal synthesis, sintering and characterization of nano La-manganite perovskite doped with Ca or Sr, Ceramics International, 45 (2019) 4894-4901.
[82] Z. Shao, G. Xiong, J. Tong, H. Dong, W. Yang, Ba effect in doped Sr(Co0.8Fe0.2)O3-δ on the phase structure and oxygen permeation properties of the dense ceramic membranes, Separation and Purification Technology, 25 (2001) 419-429.
[83] M.T. Colomer, E. Chinarro, A.L. Ortiz, Processing and electrical conductivity of non-stoichiometric lanthanum strontium manganite perovskites prepared from powders synthesized by a polymerizable-complexation route, Ceramics International, 44 (2018) 13389-13395.
[84] S.N. Victoria, S. Ramanathan, Effect of potential drifts and ac amplitude on the electrochemical impedance spectra, Electrochimica Acta, 56 (2011) 2606-2615.
[85] R. Siqueira Melo, S. Louise, L. Carvalho, L. Reznik, Using Electrochemical Impedance Spectroscopy Sinusoidal Potential Amplitude to Assess the Efficiency of Niobium Oxide Based Organic Coating in Oil Wells Produced Water, International journal of electrochemical science, 11 (2016) 10511-10521.
[86] C. Sikalidis, Advances in Ceramics: Synthesis and Characterization, Processing and Specific Applications, IntechOpen, 2011.
[87] A. Jun, J. Kim, J. Shin, G. Kim, Optimization of Sr content in layered SmBa1–xSrxCo2O5+δ perovskite cathodes for intermediate-temperature solid oxide fuel cells, International Journal of Hydrogen Energy, 37 (2012) 18381-18388.
[88] M. Yuan, W. Dong, L. Wei, Q. Liu, Y. Meng, X. Wang, B. Wang, B. Zhu, Stability study of SOFC using layered perovskite oxide La1·85Sr0·15CuO4 mixed with ionic conductor as membrane, Electrochimica Acta, 332 (2020) 135487.
[89] J.A.M. Van Roosmalen, E.H.P. Cordfunke, The Defect Chemistry of LaMnO3±δ: 3. The Density of (La,A)MnO3+δ (A = Ca, Sr, Ba), Journal of Solid State Chemistry, 110 (1994) 106-108.
[90] K. Nakamura, M. Xu, M. Kläser, G. Linker, Excess Oxygen in Low Sr Doping La1−xSrxMnO3+δ Epitaxial Films, Journal of Solid State Chemistry, 156 (2001) 143-153.
[91] Y. Choi, M.E. Lynch, M.C. Lin, M. Liu, Prediction of O2 Dissociation Kinetics on LaMnO3-Based Cathode Materials for Solid Oxide Fuel Cells, The Journal of Physical Chemistry C, 113 (2009) 7290-7297.

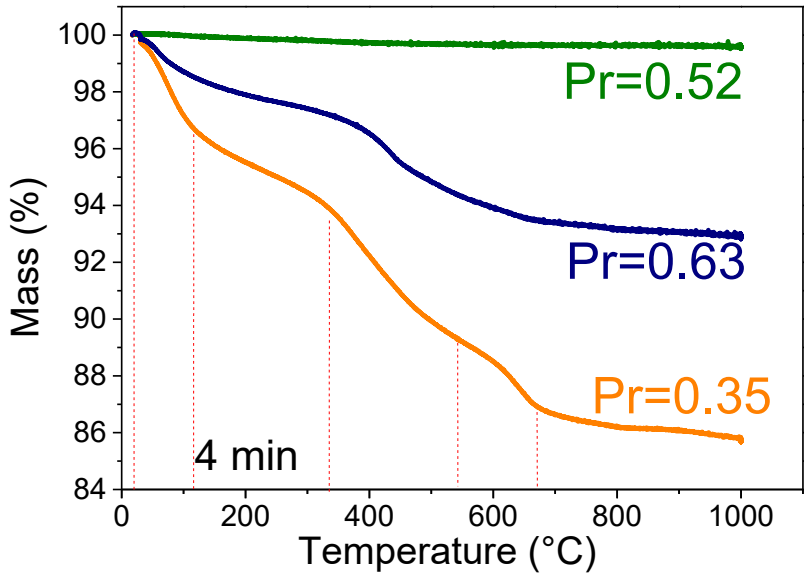

Figure 1. Thermogravimetric Analysis the as-synthesized La0.7-xPrxCa0.3MnO3 perovskites (x=0.35, 0.52 and 0.63) in the temperature range from room temperature to 1000 °C.

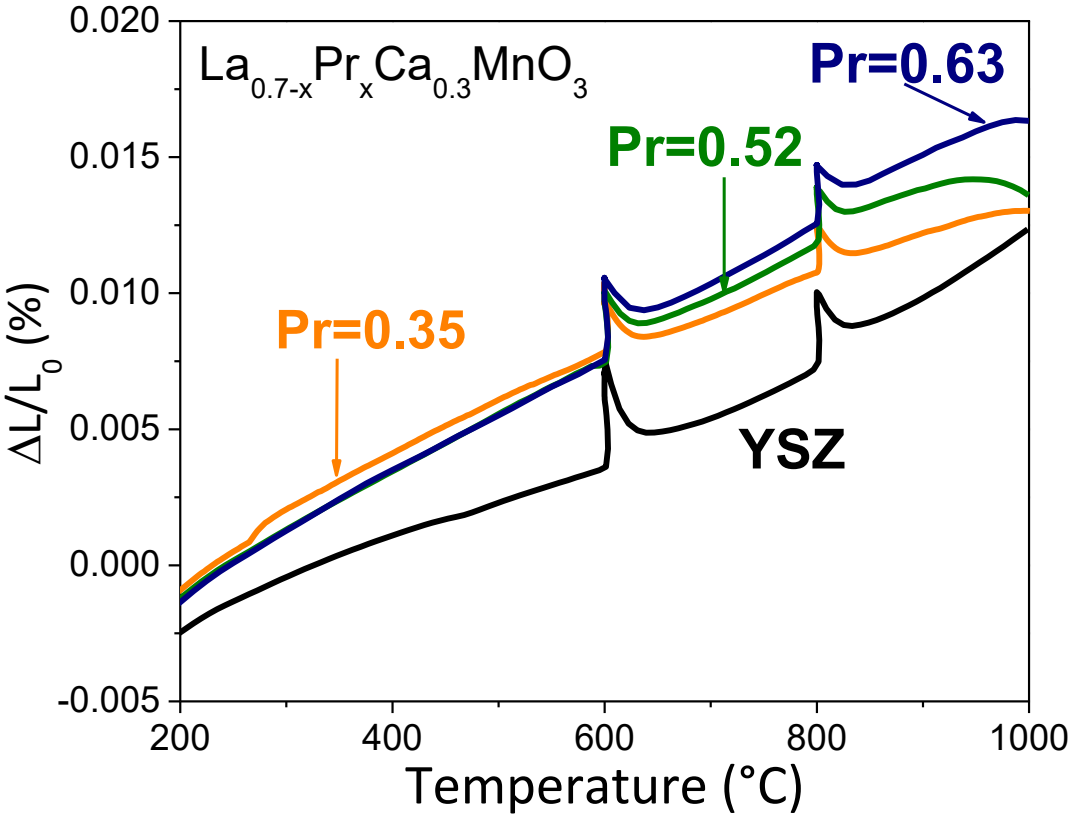

Figure 2. Thermal expansion coefficient activities of LPCM perovskite pellets synthesized at 4 min. **For comparison, TEC plot of the YSZ pellets after a sintering process at 1500 °C is also presented.**

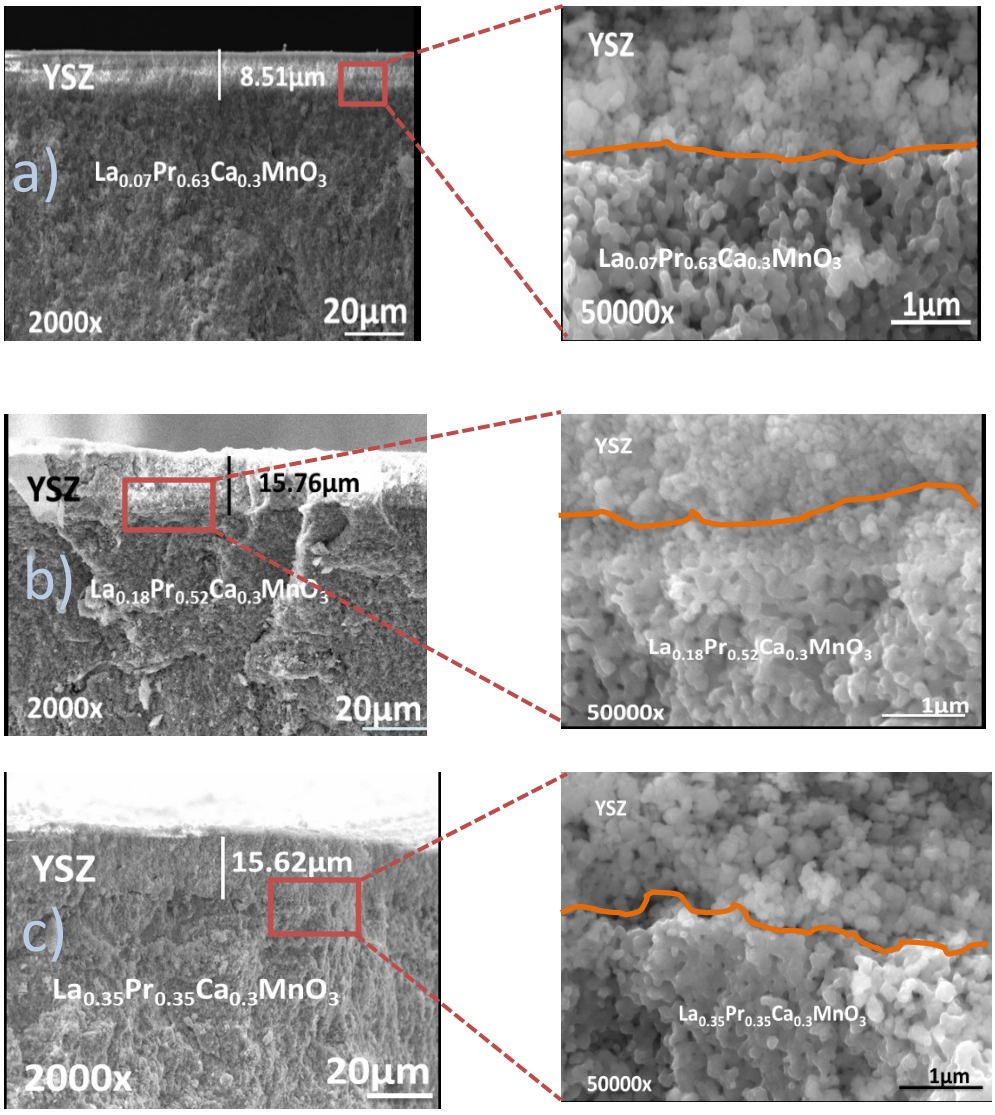

Figure 3. SEM cross- section images of the cathode/YSZ systems. The micrographs show a magnification of two different sections showing the cathode and electrolyte morphologies: a) Pr=0.63 b) Pr=0.52 and d) Pr=0.35. The samples were synthesized using a reaction time of 4 min followed by a sintering process at 1000 °C.

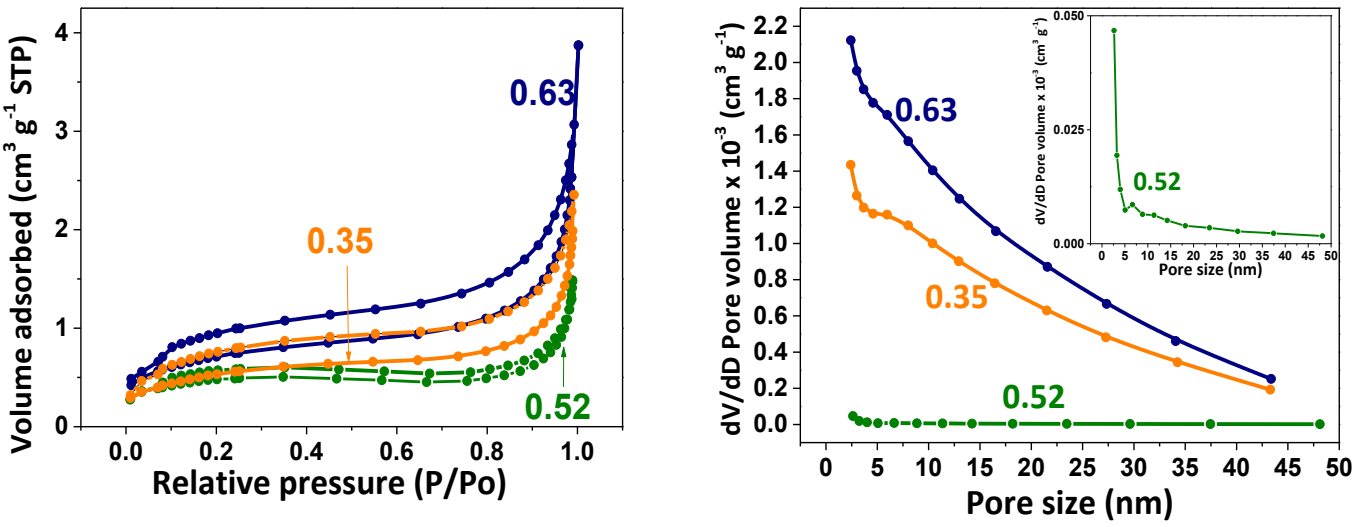

Figure 4. a) Nitrogen adsorption-desorption isotherms (BET) of the as-prepared LPCM/YSZ systems and b) pores size distribution measured by BJH method.

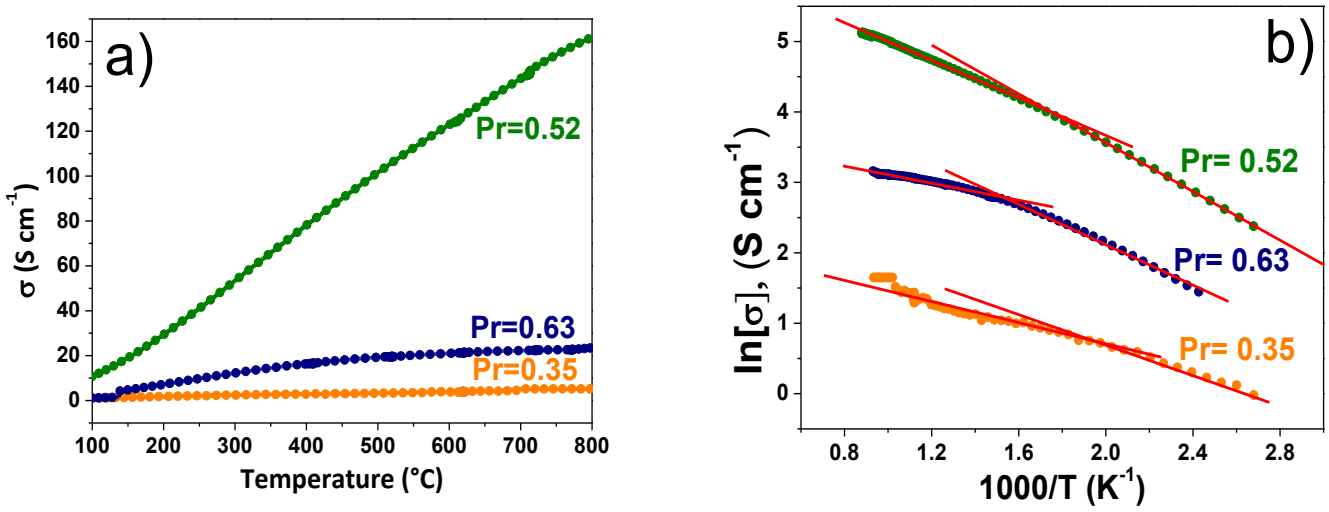

Figure 5. a) Direct electrical conductivity vs temperature and b) Arrhenius plots of LPCM/YSZ perovskites synthesized by microwave irradiation method at 4 min of reaction time. The measurements were characterized in air.

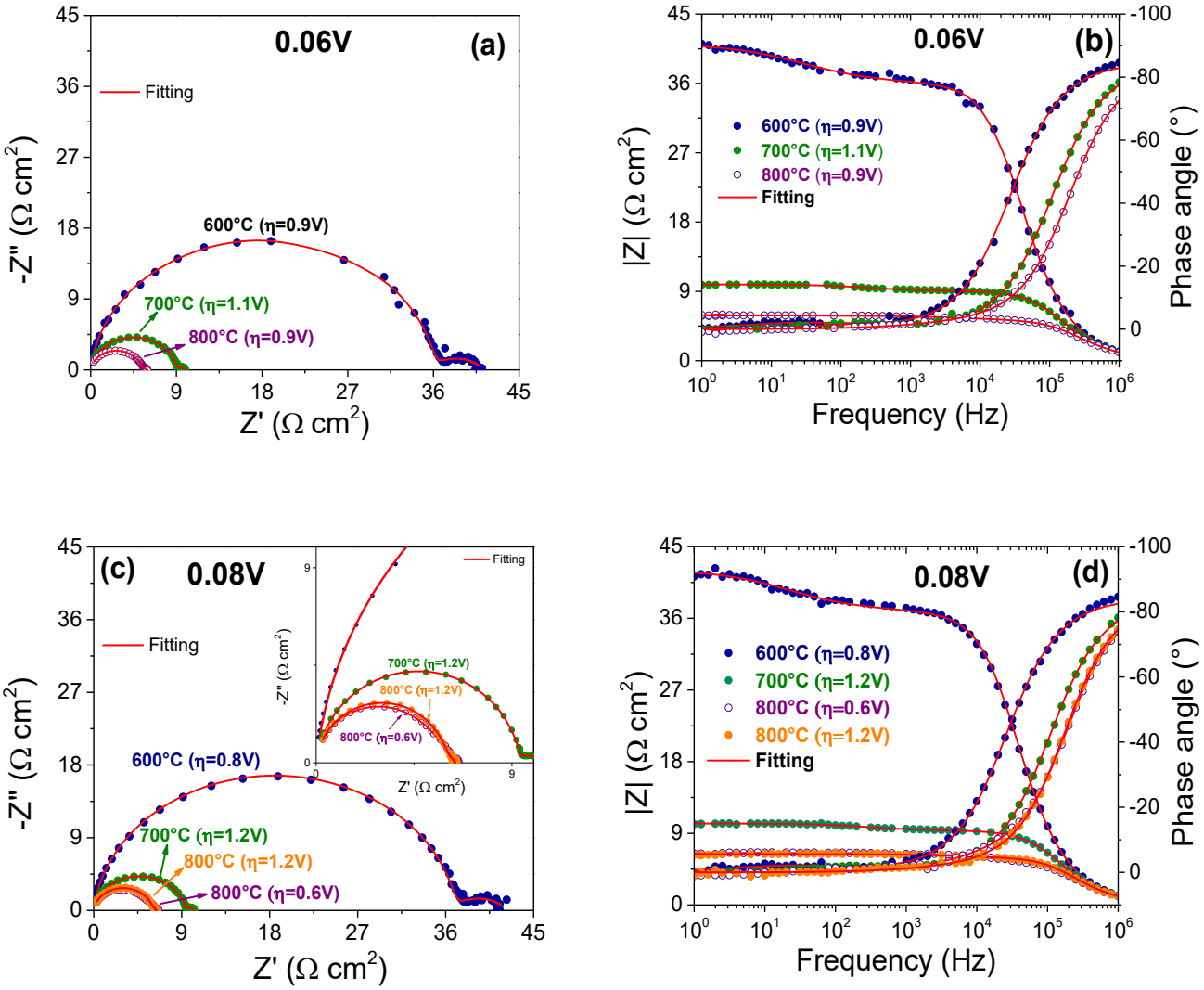

Figure 6. EIS spectra in air of the $La_{0.07}Pr_{0.63}Ca_{0.3}MnO_3$/ YSZ systems at 600, 700 and 800 °C with an amplitude of 0.06 V using a frequency range of 10^0-10^6 Hz.

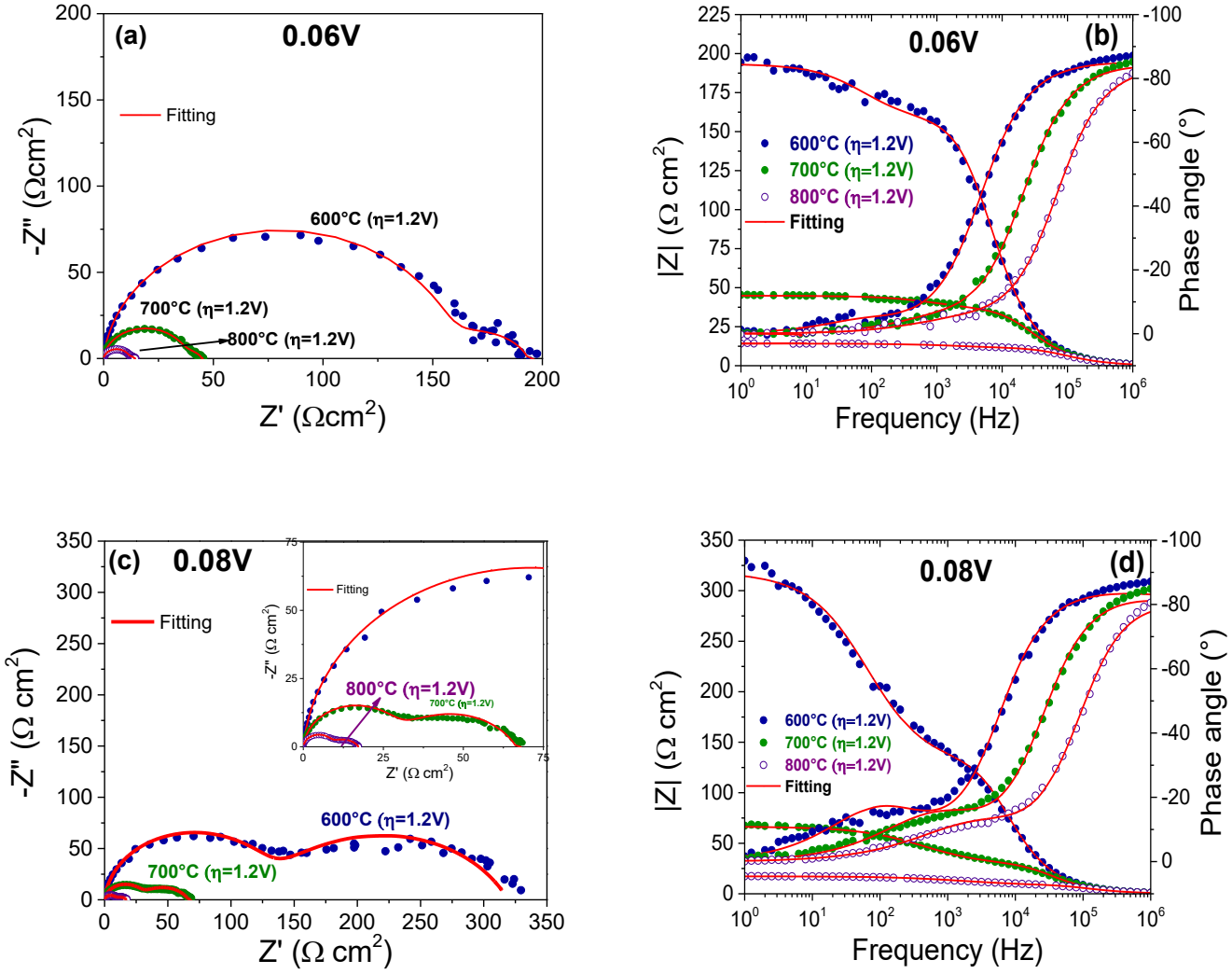

Figure 7. EIS spectra in air of the $La_{0.35}Pr_{0.35}Ca_{0.3}MnO_3$ /YSZ systems at 600, 700 and 800 °C with an amplitude of 0.08 V using a frequency range of 10^0-10^6 Hz.

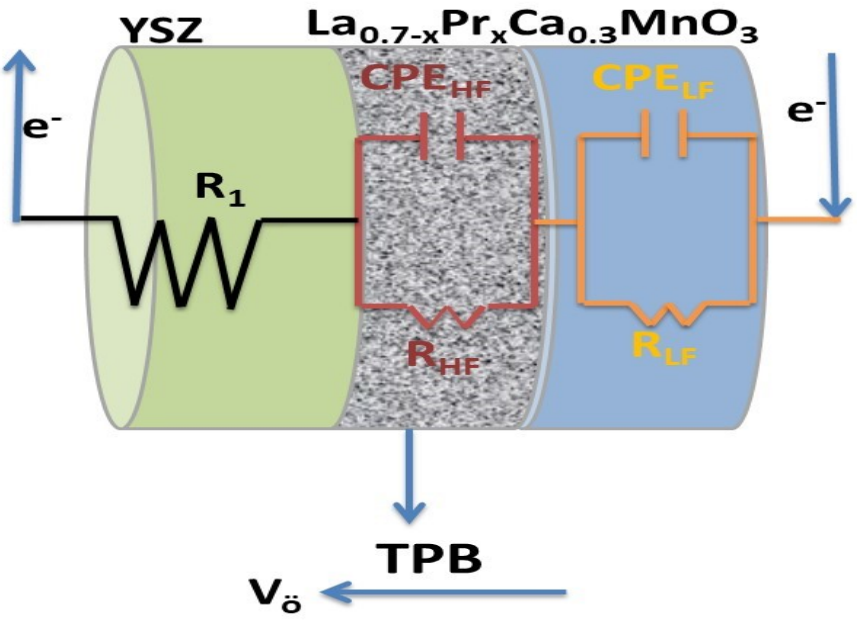

(a)

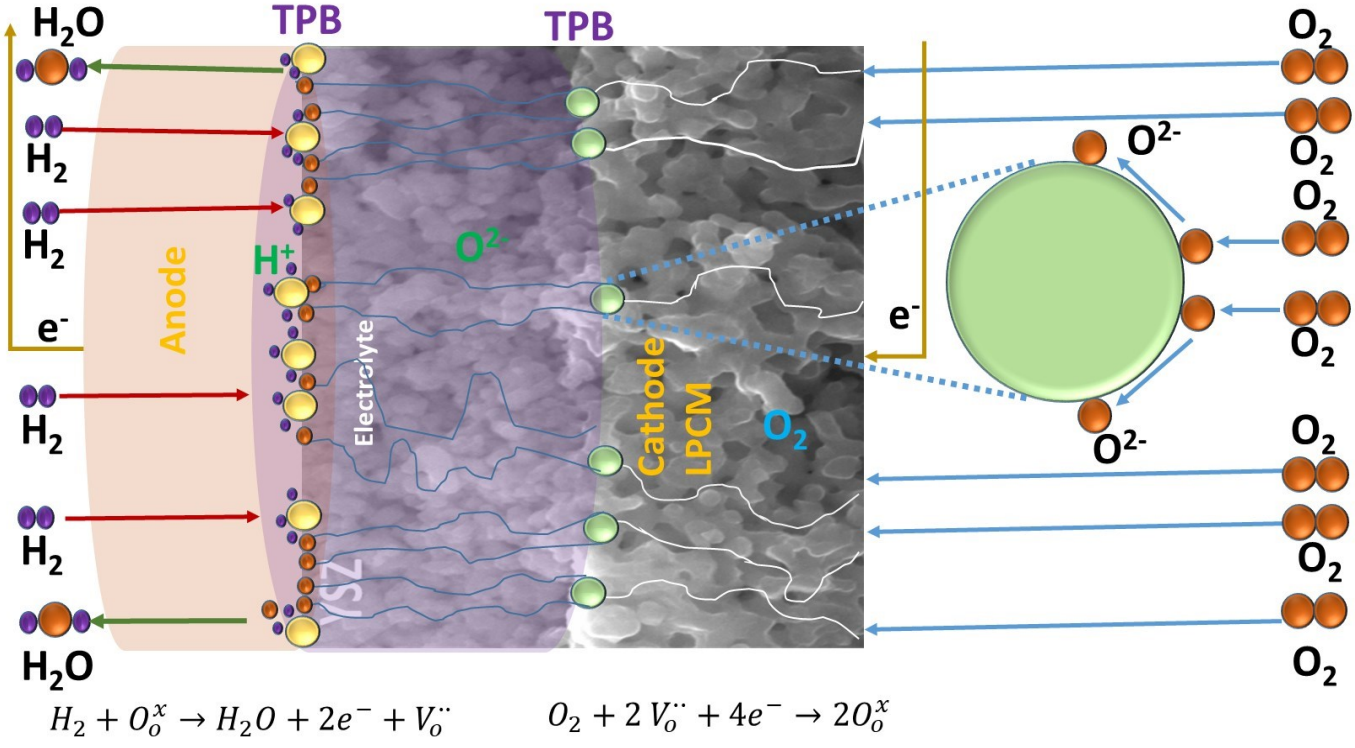

$H_2 + O_o^x \rightarrow H_2O + 2e^- + V_o^{\cdot\cdot}$ $O_2 + 2\,V_o^{\cdot\cdot} + 4e^- \rightarrow 2O_o^x$

(b)

Figure 8. a) Equivalent circuit used for experimental fitting and b) schematic representation of the ionic conduction pathway.

Table 1. Resistance and CPE contributions of the LPCM/YSZ pellet **synthesized at** 4 min

Pr =0.63

Temperature	Amplitude	η	R_1 (10^{-3})	R_{HF}	CPE_{HF}		R_{LF}	CPE_{LF}		σ (10^{-3})	χ^2 (10^{-3})
					Y_{oHF} (10^{-7})	n_{HF}		Y_{olF}(10^{-3})	n_{LF}		
(°C)	(V)	(V)	(Ω cm^2)	(Ω cm^2)	($Ω^{-1}cm^{-2}s^n$)		(Ωcm^2)	($Ω^{-1}cm^{-2}s^n$)		(S cm^{-1})	
600	0.06	0.9	0.97	36.02	3.17	0.95	5.19	8.1	0.62	2.84	3.59
	0.08	0.8	0.97	36.89	3.45	0.94	5.30	8.51	0.63	2.77	1.18
700	0.06	1.1	0.97	9.07	3.61	0.94	0.83	4.89	0.75	11.81	0.61
	0.08	1.2	0.48	9.36	3.63	0.94	0.88	4.08	0.77	11.43	0.45
800	0.06	0.9	0.48	5.17	3.45	0.94	0.69	1.88	0.62	19.97	0.91
	0.08	0.6	0.45	5.08	2.99	0.96	1.46	0.22	0.68	17.88	2.94
	0.08	1.2	0.26	5.93	2.98	0.95	0.46	1.66	0.69	18.31	2.88

Pr =0.35

Temperature	Amplitude	η	R_1 (10^{-3})	R_{HF}	CPE_{HF}		R_{LF}	CPE_{LF}		σ (10^{-4})	χ^2 (10^{-3})
					Y_{oHF} (10^{-7})	n_{HF}		Y_{olF}(10^{-3})	n_{LF}		
(°C)	(V)	(V)	(Ω cm^2)	(Ω cm^2)	($Ω^{-1}cm^{-2}s^n$)		(Ωcm^2)	($Ω^{-1}cm^{-2}s^n$)		(S cm^{-1})	
600	0.06		2.53	157.2	3.49	0.95	36.36	2.74	0.76	6.0	3.54
	0.08	**1.2**	2.53	217.17	3.18	0.97	95.66	0.77	0.72	3.7	4.97
700	0.06		2.53	36.06	3.67	0.95	8.79	2.10	0.73	26.1	2.57
	0.08		1.27	45.30	3.28	0.97	21.23	1.29	0.68	17.6	3.69
800	0.06		1.27	11.11	3.82	0.95	3.08	5.99	0.66	82.4	2.31
	0.08		1.27	8.14	3.35	0.97	9.16	3.41	0.63	67.6	1.83